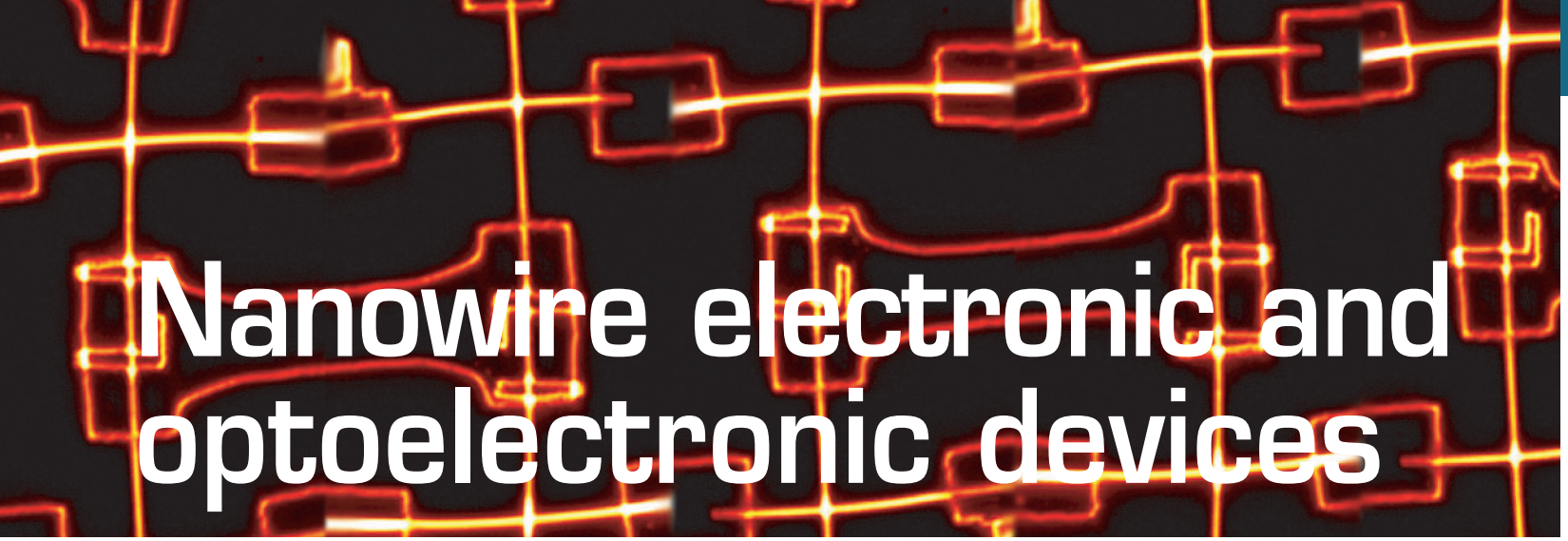

Nanowire electronic and optoelectronic devices

Electronic and optoelectronic devices impact many areas of society, from simple household appliances and multimedia systems to communications, computing, and medical instruments. Given the demand for ever more compact and powerful systems, there is growing interest in the development of nanoscale devices that could enable new functions and/or greatly enhanced performance. Semiconductor nanowires are emerging as a powerful class of materials that, through controlled growth and organization, are opening up substantial opportunities for novel nanoscale photonic and electronic devices. We review the broad array of nanowire building blocks available to researchers and discuss a range of electronic and optoelectronic nanodevices, as well as integrated device arrays, that could enable diverse and exciting applications in the future.

Yat Li, Fang Qian, Jie Xiang, and Charles M. Lieber*

Department of Chemistry and Chemical Biology, Division of Engineering and Applied Sciences, Harvard University, 12 Oxford Street, Cambridge, MA 02138, USA

**E-mail: cml@cmliris.harvard.edu*

Semiconductor nanowires (NWs)[1-8], nanocrystals[9-11], and carbon nanotubes[12-17] offer many opportunities for the assembly of nanoscale devices and arrays by the bottom-up paradigm[1-4]. Moreover, these nanomaterials demonstrate new and/or enhanced functions crucial to many areas of technology. Central to realizing applications through a bottom-up paradigm is the rational control of key nanomaterial parameters, including chemical composition, structure, size, morphology, and doping. It is these parameters that determine, for example, electronic and optoelectronic properties critical to predictable device function. Significantly, semiconductor NWs represent the nanomaterial system where these key parameters have been best controlled to date.

First, an underlying conceptual framework has been developed to enable the growth of nanowires of virtually any uniform composition and structure, with the wide range of reported nanowires confirming these models. Second, in many cases controlled *p*- and *n*-type doping, which is critical to almost any active device application, has been demonstrated. Third, the control over nanowire growth has enabled the

ISSN:1369 7021 © Elsevier Ltd 2006

creation of a host of structures with modulated structure and/or doping, including axial and radial heterostructures, which allows function to be 'built-in' at the nanoscale without the need of lithography, which dominates many top-down technologies.

In this article, we review progress in the area of NW growth, the fundamental electronic and optoelectronic properties of semiconductor NWs and NW heterostructures, as well as strategies for and emerging results demonstrating their promise as nanoscale electronic and photonic devices and device arrays.

Semiconductor nanowires

At the heart of the success of NWs as versatile building blocks for nanoscience is the development of a general strategy for the controlled growth of these materials[1-4,18]. We first reported that metal nanoparticles could be used as 'catalysts' within the general context of the vapor-liquid-solid growth[19,20] to control the critical nucleation and subsequent elongation steps of NW growth[18]. Using this approach, we showed early on that a broad range of NWs with homogeneous composition and single-crystal structures could be prepared as summarized in Fig. 1[18,21-36]. In addition, this earlier work on homogenous NW materials demonstrates that NW diameter is indeed controlled by the size of the nanoparticle 'catalyst', as suggested by the growth model[18], with diameters as small as 3 nm realized[34]; that NW length is proportional to growth time[28]; and, significantly, that specific dopants can be incorporated into NWs to control their electronic properties[22,27,29,31,33,35,36]. The ability to control the fundamental electronic properties of NWs through doping has been central to much of our success in developing active electronic and optoelectronic nanodevices.

Another critical breakthrough in the development of NW building blocks has been the recent demonstration of controlled growth of axial[37-39] and radial heterostructures[40-46], where the composition and/or doping is modulated down to the atomic level along or perpendicular to the axes of NWs, respectively (Fig. 1). The growth of both types of heterostructure is possible because of our understanding of the growth mechanism first defined for homogeneous NW structures. In the case of axial heterostructures, one or more heterojunctions are created within the NW by alternating the flow of different reactants and/or dopants; this sequence can be repeated to make an arbitrary number of junctions[37-39]. In the case of radial NW heterostructures[40-46], after growth and elongation of a crystalline NW core, conformal radial shell growth is carried out by altering the conditions to favor homogeneous deposition on the NW surface versus reactant addition at the nanoparticle catalyst. Subsequent introduction of different reactants and/or dopants produces multiple shell structures of nearly arbitrary composition. The ability to prepare controlled and diverse axial and radial heterostructures sets NWs apart from other nanomaterials, such as carbon nanotubes, and as discussed below represents a substantial advantage for the development of increasingly

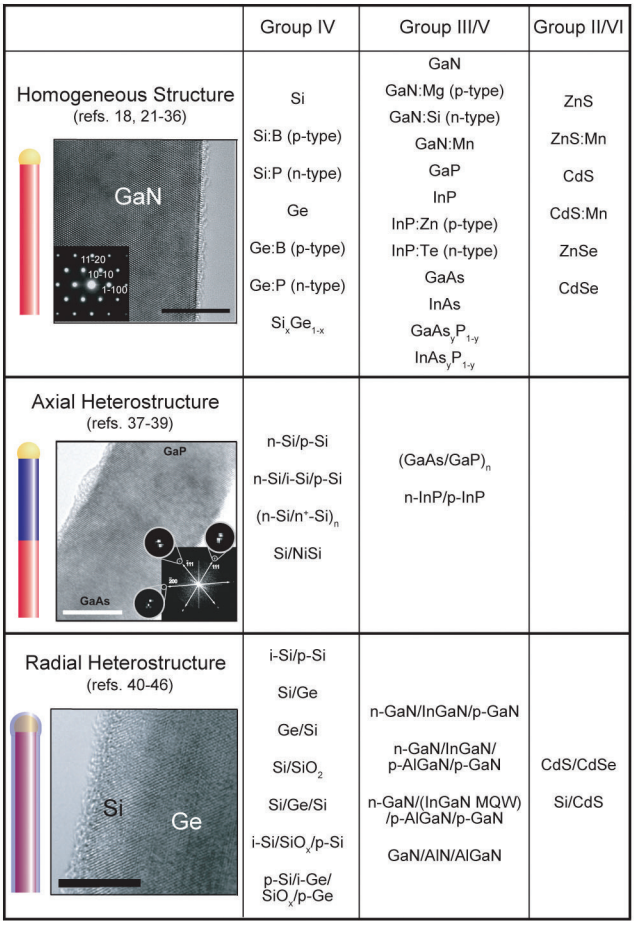

Fig. 1 Semiconductor NWs and NW heterostructures. (Left) Structural schematics and representative transmission electron microscopy (TEM) images of uniform single-crystal semiconductor NWs, axial NW heterostructures, and radial (core/shell, core/multi-shell) NW heterostructures. Scale bars are all 10 nm. (Right) Summary of NW materials demonstrated by our group within these three distinct categories.

powerful and unique nanoscale electronic and optoelectronic devices crucial to future applications.

Nanowire field-effect transistors

Homogeneous doped NWs represent key building blocks for a variety of electronic and optoelectronic devices. A prototypical example of such a device with broad potential for applications is the NW field-effect transistor (FET) and, moreover, studies of FETs enable evaluation of the performance level of NWs compared with corresponding planar devices. We have shown that representative NW materials including Si[22,30,35,47], Ge[33], and GaN[29,31] can be prepared with complementary *n*- and *p*-type doping. For example, studies of NWFETs fabricated from boron-[47] (phosphine-[35]) doped SiNWs have shown that the devices are turned on as the gate voltage becomes more negative (positive), characteristic of *p*- (*n*-) channel FETs (Figs. 2a, b). Importantly, analysis of these results has demonstrated that our doped Si, Ge, and GaN

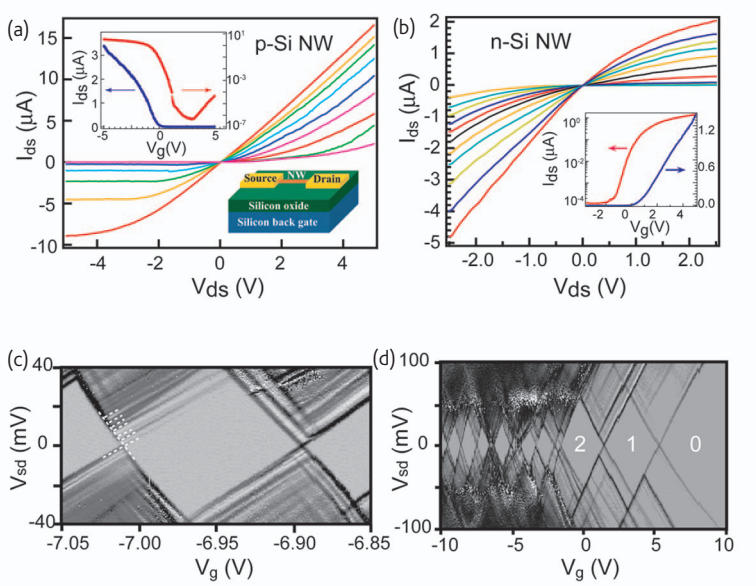

Fig. 2 Si NWFETs: family of current versus drain-source voltage (I_{ds}-V_{ds}) plots for a representative (a) 20 nm p-Si NW array device (channel length of 1 μm; from red to pink, V_g = -5 V to 3 V); and (b) 20 nm n-Si NW device (channel length of 2 μm; from yellow to red, V_g = -5 V to 5 V) in a standard back-gated NWFET geometry as illustrated. Insets in (a) and (b) are current versus gate-voltage (I_{ds}-V_g) curves recorded for NWFETs plotted on linear (blue) and log (red) scales at V_{ds} = -1 V and 1 V, respectively. (c) dI/dV_{sd}-V_{sd}-V_g data recorded at 1.5 K on a 3 nm diameter Si NW device in the Coulomb blockade regime with 100 nm channel length. Dark lines (peaks in dI/dV_{sd}) running parallel to the edges of the diamonds correspond to individual excited states and are highlighted by white dashed lines. (d) dI/dV_{sd}-V_{sd}-V_g data for a Si NW device with diameter of 3 nm and channel length of 50 nm at 4.2 K. The carriers are completely depleted for V_g > 5.5 V, below which carriers are added consecutively to the dot and the first three carriers are labeled as 0, 1, and 2. (Reprinted with permission from[35,47,50]. © 2004 Wiley-VCH and 2004, 2005 American Chemical Society, respectively.)

NWFETs can exhibit performance comparable to the best reported for planar devices made from the same materials. Studies have also demonstrated the high electron mobility of epitaxial InAs NWFETs with a wrap-around gate structure[48]. This conclusion is significant since the NWFETs are fabricated using nontraditional methods (e.g. solution assembly), which opens up opportunities in areas not possible with traditional single-crystal wafer-based electronics and optoelectronics.

The high performance of these homogeneous NW devices has been further verified by low-temperature measurements. For example, proximity-induced superconductivity has been realized in InAs NWs contacted with Al-based superconductor electrodes[49]. The results indicate Schottky barrier-free contacts between NWs and metals, and show that the phase-coherence length for electron propagation in these NWs is up to hundreds of nanometers. Our group has also demonstrated that molecular-scale SiNW devices[50] configured as single-electron transistors exhibit single period Coulomb blockade oscillations (Fig. 2c) and coherent transport through single NW 'islands' for lengths up to 400 nm. This result shows that Si NWs are a clean system with little or no structural/dopant variation on this length scale. In contrast, lithographically defined Si NWs have much greater structural and/or dopant fluctuations and yield a length scale for electronically distinct regions that is over an order of magnitude smaller[51]. Notably, coherent transport has been observed in molecular-scale SiNWs down to the last few charges (Fig. 2d)[50], which further demonstrates the high quality of the NW material, long carrier mean-free-paths, and the potential to serve as a unique building block for both low- and room-temperature applications.

Applications of NWFETs

An attractive feature of NWFETs is that there is a separation of the high-temperature growth processes, which are used to prepare high-quality single-crystalline material, and the low-temperature assembly and contact deposition, which enables rapid design and fabrication of a host of single- and multi-NW device structures on virtually any substrate[2-4]. Two distinct applications of this key concept include the development of high-performance, multi-NW devices and circuits on noncrystalline substrates[47,52,53] and arrays of single-NWFETs for sensing[54-59]. In addition to our initial demonstration that NWFETs and inverters can be configured on flexible plastics with properties comparable to high-performance single-crystal planar devices[52], we have recently shown that it is possible to assemble more complex ring-oscillator circuits (Fig. 3a) by simple fluid-based assembly and patterning[53]. The necessary on-chip device integration is achieved during fabrication without the need for external wiring because of the high-reproducibility of SiNW FETs. Significantly, characterization of these NW ring oscillators demonstrates very stable and self-sustained output voltage oscillations with a frequency of 11.7 MHz (Fig. 3b), which is substantially better than organic and amorphous semiconductor devices processed at low temperatures[53].

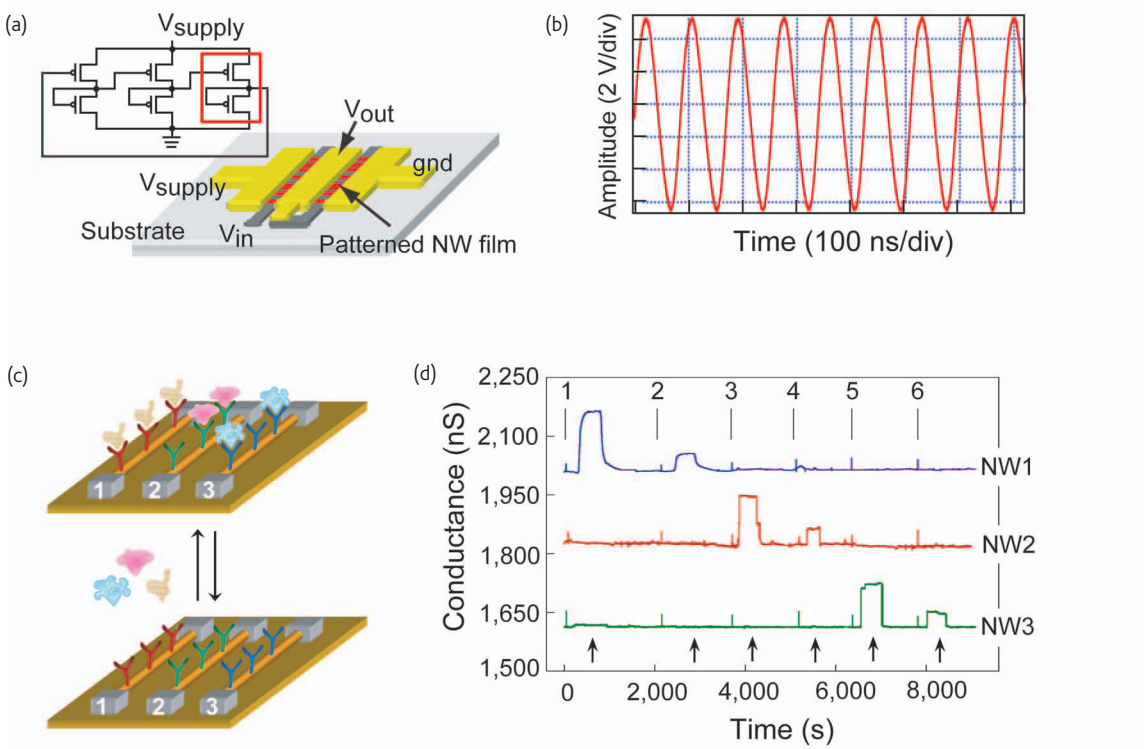

Fig. 3 Applications of Si NWFETs. (a) Schematic of a multi-NW inverter on a glass substrate and a circuit diagram for a NW ring oscillator consisting of three inverters in series. (b) Oscillation at 11.7 MHz for a p-Si NW ring oscillator with V_{supply} = 43 V. (c) Schematic illustrating multiplexed protein detection by three Si NW devices in an array. Devices 1, 2, and 3 are made of similar NWs, which are then selectively functionalized with distinct monoclonal receptors (1, red; 2, green; 3, blue) specific to three different cancer markers. (d) Conductance versus time data recorded for the simultaneous detection of prostate specific antigen (PSA), carcinoembryonic antigen (CEA), and mucin-1 on a p-Si NW array in which NW1, NW2, and NW3 were functionalized with monoclonal receptors for PSA, CEA, and mucin-1, respectively. The protein solutions were delivered sequentially to the NW array as follows: (1) 0.9 ng/ml PSA, (2) 1.4 pg/ml PSA, (3) 0.2 ng/ml CEA, (4) 2 pg/ml CEA, (5) 0.5 ng/ml mucin-1, and (6) 5 pg/ml mucin-1. Buffer solutions were injected following each protein solution at points indicated by black arrows. (Reprinted with permission from[53,58]. © 2005 Nature Publishing Group.)

In addition, NWFETs have emerged as extremely powerful sensors for ultrasensitive, direct, label-free detection of biological and chemical species[54-59]. Binding to the surface of an NWFET is analogous to applying a gate voltage, which leads to the depletion or accumulation of carriers and subsequent changes in the NW conductance (Fig. 3c). The small diameters and high performance of NWFETs yield high sensitivity, with the detection of single virus particles representative of their unique power[56]. NWFET sensors can also be readily integrated into electrically addressable sensor arrays, which demonstrate multiplexed, real-time detection of multiple disease marker proteins at the femtomolar level (Fig. 3d)[58]. This work offers potential for powerful sensors that could significantly improve healthcare in the future.

Crossed NW structures

NW building blocks and device architectures more complex than the NWFETs described above can open up new opportunities that differentiate NW-based devices from conventional paradigms. The crossed NW architecture that we introduced in 2001[27,60] is a clear example since the key device properties are defined by assembly of the two nanowire components and not by lithography. Hence, the dimensions of the crossed NW device are limited only by the NW diameters, which makes the architecture readily scalable for high-density integration and, depending on the choice of NWs, the structure can yield a variety of critical device elements, including transistors and diodes[27,60]. For example, crossed NWFETs can be configured from one NW as the active channel and the second crossed NW as the gate electrode separated by a thin SiO_2 dielectric shell on the SiNW surface, with the gate on the surface of one or both of the crossed NWs[60]. This concept was first demonstrated using Si NWs as the channel and GaN NWs as the gate electrodes, including the integration of multiple crossed NWFETs on a single Si NW channel to demonstrate both NOR logic-gate structures (Fig. 4a) and basic computation[60]. More recently, we extended the idea of crossed NWFETs to demonstrate a general approach for uniquely addressing a large array of NW devices. Selective chemical modification is used to differentiate specific cross points in a four-by-four crossed Si NWFET array (Fig. 4b), thus allowing selective addressing of the four individual outputs (Fig. 4c)[61]. Significantly, these results provide a proof-of-concept that assembled crossed NW arrays can serve as the basis for addressable integrated nanosystems in which signals are restored at the nanoscale.

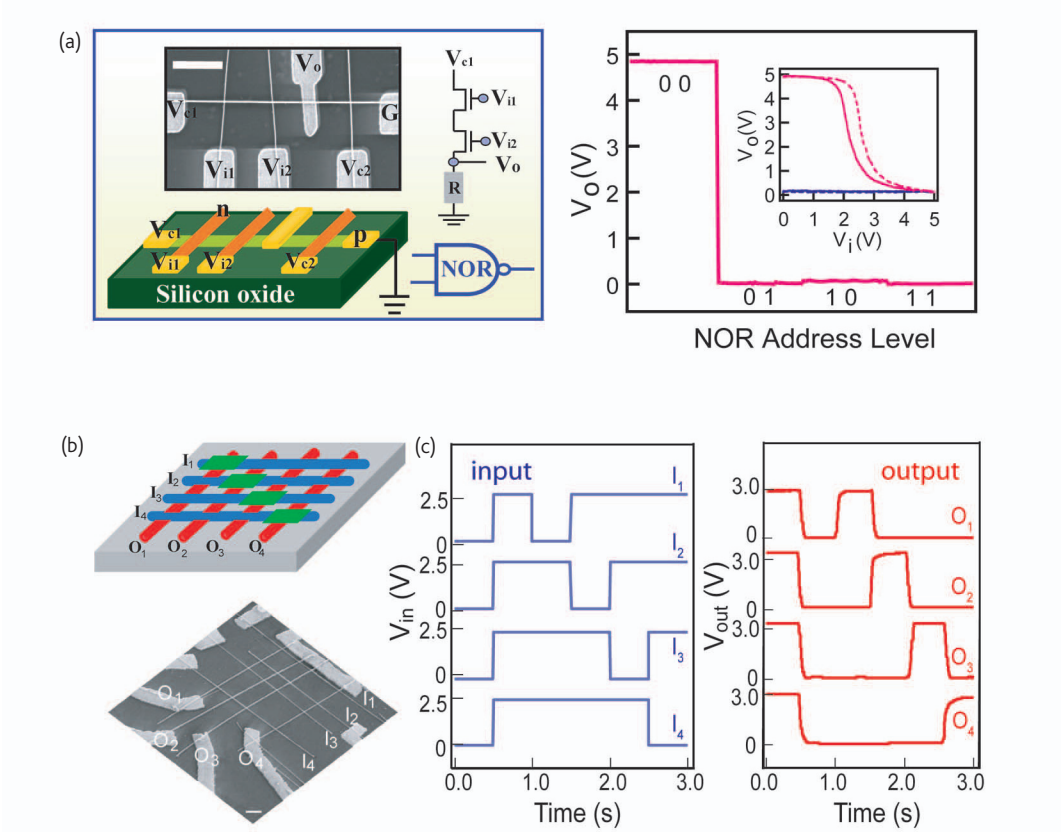

Fig. 4 Crossed NW electronic devices. (a, left) Schematic of a logic NOR gate constructed from a one-by-three crossed NW junction array using one SiNW and three GaN NWs; insets show a representative scanning electron micrograph of the device (scale bar, 1 μm) and symbolic electronic circuit. (a, right) Output voltage versus the four possible logic address level inputs; inset is the V_o-V_i relation, where the solid and dashed red (blue) lines correspond to V_o-V_{i1} and V_o-V_{i2} when the other input is 0 (1). (b) Schematic and scanning electron micrograph of a four-by-four crossed Si NW array address decoder, with four horizontal NWs (I_1 to I_4) as inputs and four vertical NWs (O_1 to O_4) as signal outputs. The four diagonal cross points in the array were chemically modified (green rectangles) to differentiate their responses from to the input gate lines. Scale bar, 1 μm. (c) Real-time monitoring of the V_g inputs (blue) and signal outputs (red) for the four-by-four decoder. (Reprinted with permission from[60,61]. © 2001 and 2003 American Association for the Advancement of Science, respectively.)

The crossed NW concept has also been used to create nanoscale *p*-*n* diodes by crossing *p*- and *n*-type NWs[27,31,52,60,62]. This concept was first demonstrated for *p*-*n* crossed InP NW junctions[27] and subsequently extended to crossed NW *p*-*n* diode junctions with *p*-Si/*n*-GaN[60], *p*-GaN/*n*-GaN[31], and other systems. Transport measurements have shown that nanoscale junctions formed in this way exhibit the expected rectifying behavior and, moreover, band-edge emission at the nanoscale cross-points in forward bias (Fig. 5a). Significantly, the capability to assemble a wide range of different *n*-type direct band-gap NWs, including GaN (ultraviolet), CdS (green), and CdSe (near infrared), with *p*-type Si NWs as a common *p*-type indirect bandgap material[62] has enabled the facile creation of multicolor light-emitting diodes (LEDs) on a single substrate in a manner not possible with conventional planar technology.

Our concept for crossed NW architecture was further generalized to hybrid devices consisting of *n*-type CdS NWs assembled onto *p*-type Si electrodes defined in heavily *p*-doped planar substrates (Fig. 5b)[63]. When the injection current increases above the threshold, these hybrid NW devices show a superlinear increase in the electroluminescence (EL) intensity at the end of the nanowire, as well as simultaneous peak narrowing to a single mode emission with instrument-resolution-limited width, corresponding to the first demonstration of a nanoscale electronic injection laser (Fig. 5c).

In addition to nanoscale light sources, crossed NW *p*-*n* junctions can also be configured as photodetectors critical for integrated photonics. For example, we have recently demonstrated avalanche multiplication of the photocurrent in nanoscale *p*-*n* diodes consisting of crossed Si/CdS NWs (Fig. 5d)[64]. These NW avalanche photodiodes (nanoAPDs) exhibit ultrahigh sensitivity with detection limits of less than 100 photons and subwavelength spatial resolution of 250 nm. Moreover, the elements in nanoAPD arrays can be addressed independently without electrical crosstalk (Fig. 5e).

Axial NW heterostructures

The integration of device function at the nanoscale can also be carried out during NW synthesis by varying the composition and/or doping

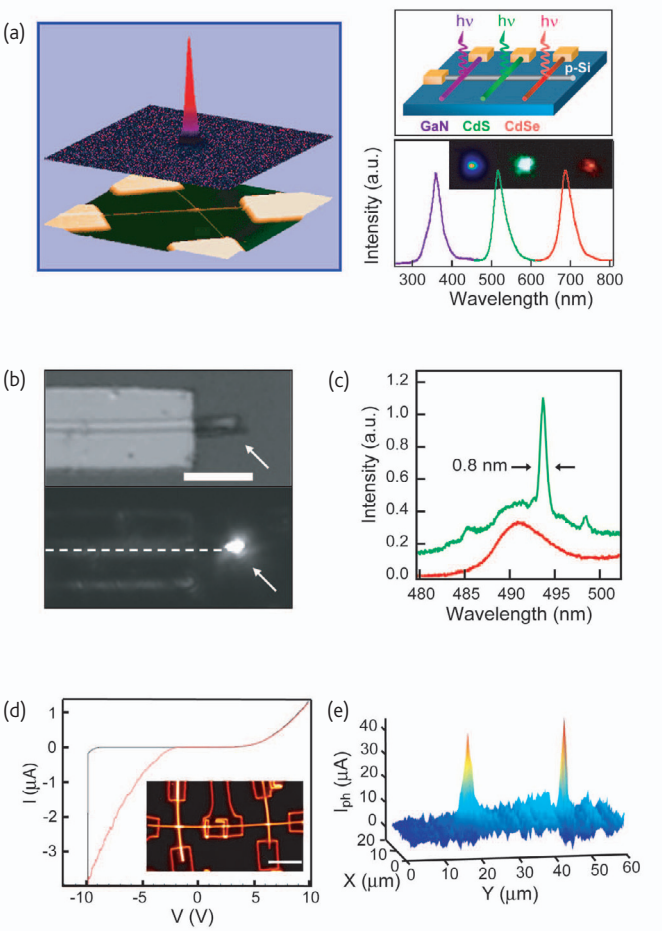

Fig. 5 Crossed NW photonic devices. (a, left) False color scanning electron micrograph of a typical n-InP/p-InP crossed NW device, overlaid with corresponding spatially resolved EL image showing the light emission from the cross point. (a, right) Schematic and EL of a tricolor nanoLED array, consisting of a common p-type Si NW crossed with n-type GaN, CdS, and CdSe NWs. (b) Optical and room-temperature EL images of a nanolaser device, fabricated by assembling n-CdS NWs on a heavily doped p-Si substrate. The dashed line highlights the NW position. Scale bar, 5 μm. (c) EL spectra obtained from the end of the nanolaser with injection currents below (200 μA, red) and above (280 μA, green) the lasing threshold. The spectra are offset by 0.10 intensity units for clarity. (d) I-V characteristic of a n-CdS/p-Si crossed NW APD in dark (black line) and under illumination (red line); inset is the optical micrograph of an array consisting of an n-CdS NW (horizontal) crossing two p-Si NWs (vertical); the larger rectangular features correspond to metal contacts. Scale bar, 10 μm. (e) Spatially resolved photocurrent measured from the NW APD array as in the inset of (d). (Reprinted with permission from[62,27,64]. © 2005 Wiley-VCH; 2003 and 2006 Nature Publishing Group, respectively.)

during axial elongation, whereby the resulting axial junctions can yield controlled nanoscale device function without the need for lithography. A representative example is a GaAs/GaP compositionally modulated axial heterostructures (Fig. 6a)[37]. Since GaAs is a direct bandgap semiconductor and GaP has an indirect bandgap, these NW heterostructures can be patterned synthetically and emit light as nanoscale barcodes. In addition, *p-n* junctions formed within individual NWs can also be prepared in a similar way. Forward biased *n*-InP/*p*-InP single NW devices function as nanoscale LEDs with light emission at the *p-n* interface as shown in Fig. 6b.

We have taken this key concept of composition modulation to define functional devices in several other directions relevant to electronic and optoelectronic devices. First, we demonstrated the selective transformation of Si NWs into metallic NiSi NWs and NiSi/Si NW heterostructures by thermal annealing as-made SiNWs with Ni (Fig. 6c)[38]. Significantly, this method yielded the first example of atomically sharp metal-semiconductor interfaces between single metallic (NiSi) and semiconductor (Si) nanowires. In these heterostructures, Si NWFET source-drain contacts are defined by the metallic NiSi NW regions, which function as excellent ohmic contacts at room temperature (Fig. 6d), and thus provide an integrated solution for nanoscale contacts and interconnects.

The concept of modulating axial doping has also been demonstrated recently for Si NWs[39], thereby providing another method for introducing rich function at the initial stage of building block synthesis. Specifically, we have reported pure axial growth of n^+-$(n$-$n^+)_N$ Si NWs with key properties, including the number, size, and period of the differentially doped regions, defined in a controllable manner during synthesis (Fig. 7a, b)[39]. The synthetic modulation of dopant concentration can be exploited for several types of nanoelectronic devices and circuits. For example, we have used arrays of modulation-doped NWs as illustrated in Fig. 7c to create address decoders (Fig. 7d). A key point of this approach is that lithography is used only to define a regular array of microscale gate wires and is not needed to create a specific address code at the nanoscale as in previous work[61]. Thus it offers the potential to break lithography barriers in ultra-dense arrays.

In addition, the synthetic control of the size and separation of modulation-doped regions can be exploited to define quantum dot (QD) structures, where the band offset caused by variations in dopant concentration produces potential barriers confining the QD[39]. Modulation-doped Si NWs having structures of the form n^+-n_1-$n_{QD}{}^+$-n_2-$n_{QD}{}^+$-n_1-n^+ (Fig. 7e, left) exhibit a single Coulomb oscillation period consistent with two weakly coupled QDs when the barrier n_2 is large and, as this barrier is reduced (through synthesis), the tunneling conductance between QDs is enhanced (Fig. 7e, right)[39]. These studies clearly demonstrate the potential of encoding functional information into NWs during synthesis, and we believe this concept will be critical for defining unique electronic and optoelectronic device capabilities in NWs compared with lithographically patterned structures.

Radial NW heterostructures

Radial composition and doping modulation in NW structures represent another approach for enhancing performance and/or enabling new function through synthesis versus lithography[40-46]. In the context of pushing the performance limits of NWFETs, we have designed and demonstrated a one-dimensional hole gas system based on an undoped

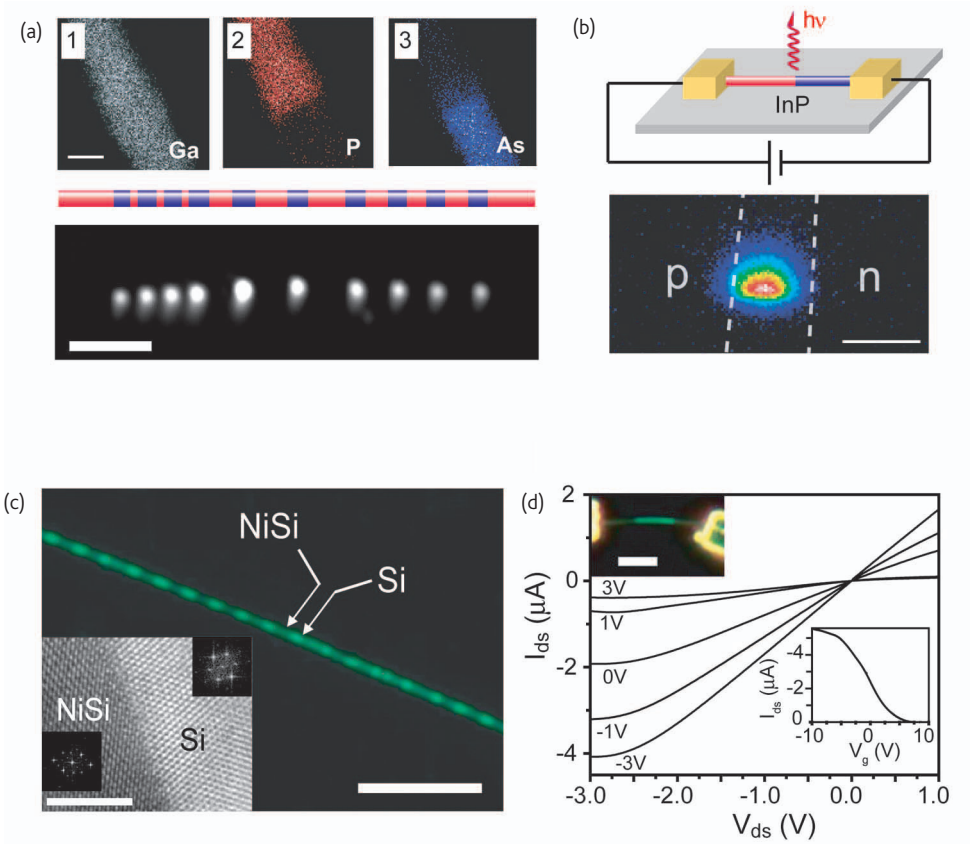

Fig. 6 Axial NW heterostructures. (a, top 1-3) TEM elemental mapping of a single GaAs/GaP nanowire heterojunction, showing the spatial distribution of Ga (gray), P (red), and As (blue) at the junction. Scale bar, 20 nm. (a, bottom) Schematic and photoluminescence (PL) image of a 21-layer, $(GaP/GaAs)_{10}GaP$, nanowire superlattice. The ten bright regions correspond to GaAs (blue, direct bandgap) regions, while the dark segments are from the GaP (red, indirect bandgap) regions. (b) Schematic of a modulation-doped InP NW LED and image of the emission from the device. Dashed white lines indicate the edges of the electrodes. Scale bar, 3 μm. (c) Dark-field optical image of a single NiSi/Si NW superlattice heterostructure. The bright green segments correspond to Si and the dark segments to NiSi; scale bar is 10 μm. Inset shows a high-resolution TEM image of the atomically abrupt interface between the NiSi and Si; scale bar is 5 nm. (d) I_{ds}-V_{ds} curves of a NiSi/p-Si/NiSi heterojunction NWFET fabricated using a 30 nm diameter p-Si NW; upper inset is a dark-field optical image of the same device showing that the contacts are made to the metallic NiSi regions only. Scale bar, 3 μm. Lower inset is the I_{ds}-V_g obtained with V_{ds} = -3 V. (Reprinted with permission from[37,38]. © 2002 and 2004 Nature Publishing Group, respectively.)

epitaxial Ge/Si core/shell structure (Fig. 8a)[44,45]. The valence band offset of ~500 meV between Ge and Si at the heterostructure interface serves as a confinement potential for the quantum well. Free holes accumulate in the Ge channel when the Fermi level lies below the valance band edge of the Ge core. Low-temperature electrical transport studies have shown distinct conductance plateaus corresponding to transport through the first four subbands in the Ge/Si NW (Fig. 8b), where the subband spacings (Fig. 8c), $\Delta E_{1,2}$ = 25 mV and $\Delta E_{2,3}$ = 30 mV, are in good agreement with calculations[44]. Notably, the conductance exhibits little temperature dependence, consistent with our calculation of reduced backscattering in this one-dimensional system, suggesting that transport is ballistic even at room temperature.

The unique transport characteristics of Ge/Si core/shell NW heterostructures make them excellent building blocks for high-performance NWFETs and potential alternatives to planar metal-oxide-semiconductor field-effect transistors (MOSFETs). We have recently demonstrated Ge/Si nanowire devices with scaled transconductance (3.3 mS/μm) and on-current (2.1 mA/μm) values that are three to four times greater than state-of-the-art MOSFETs and the highest obtained on NWFETs (Fig. 8d)[45]. Another important benchmark of transistor performance is the intrinsic delay, $\tau = CV/I$, where C is the gate capacitance, V is the power supply voltage, and I is on-current. The data again show a clear speed advantage at a given channel length, L, for the Ge/Si NWFETs versus Si p-MOSFETs (Fig. 8e). Overall, these data verify for the first time a true performance benefit of NWs, represent the best performance achieved to date in NWFET devices, and serve as a benchmark for future development.

The generality of band-structure engineering for creating NW carrier gases has been further reinforced by our recent demonstration of an electron gas in dopant-free GaN/AlN/AlGaN radial NW heterostructures[46]. Achieving both hole and electron gases is important because they are required to enable high-performance complementary

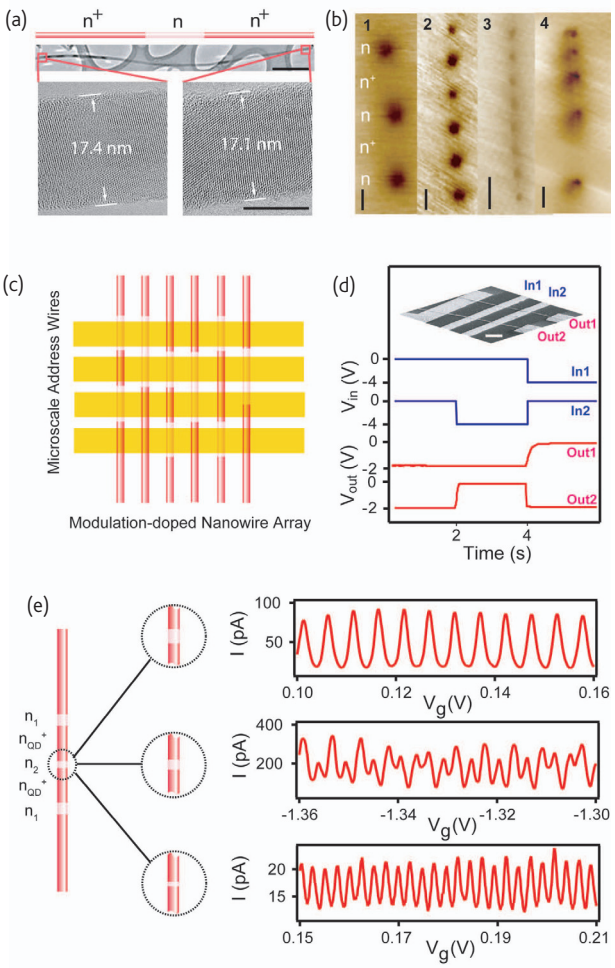

Fig. 7 Modulation-doped Si NWs and their applications. (a, top) Schematic and low-resolution TEM image of an n^+-n-n^+ modulation-doped Si NW. Scale bar, 500 nm. (a, bottom) High-resolution TEM images recorded at the two ends of the NW showing the absence of radial coating; scale bar is 10 nm. (b) Scanning gate microscopy images (1-4) of n^+-$(n$-$n^+)_N$ NWs recorded with a tip voltage of -9 V and V_{sd} = 1 V. The dark regions represent reduced conductance corresponding to lightly doped NW segments. Scale bars, 1 μm. (c) Schematic of lithography independent address decoder based on modulation-doped NW array, where microscale address wires and modulation-doped NWs serve as inputs and outputs, respectively. (d) Plots of input (blue) and output (red) voltages for the two-by-two decoder configured using two modulation-doped Si NWs as outputs (Out1 and Out2) and two Au metal lines deposited over a uniform Si_3N_4 dielectric as inputs (In1 and In2). (e, left) Schematics of a coupled double-QD structure in modulation-doped Si NW, where the n^+ QD structure is confined by two barriers from the n-type regions. The width of n_2 region between the two n^+ QDs is variable. (e, right) I-V_g data recorded at 1.5 K on three double-QD NW devices with the n_2 sections grown for 15 s, 10 s, and 5 s (top to bottom) showing different coupling. (Reprinted with permission from[39]. © 2005 American Association for the Advancement of Science.)

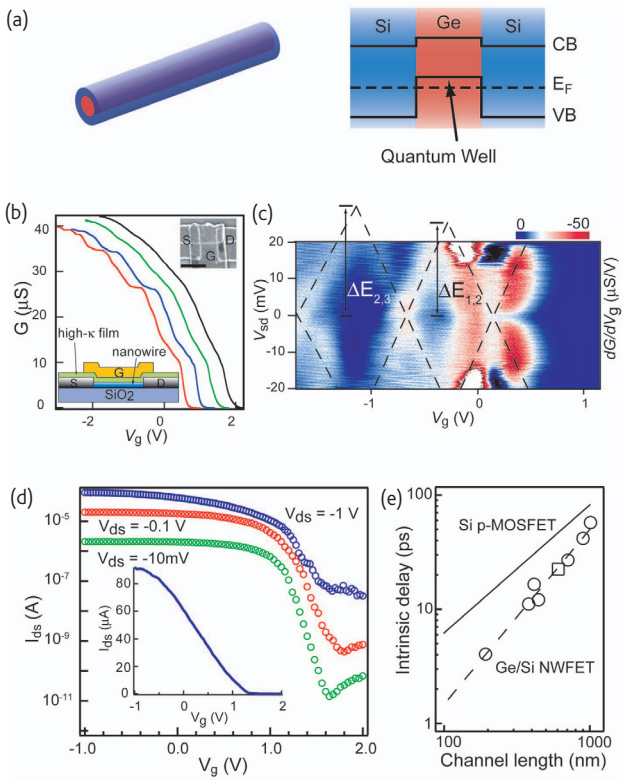

Fig. 8 Ge/Si core-shell NWFETs. (a) Schematic of an undoped Ge/Si core-shell NW and the corresponding band diagram showing the formation of a hole gas in the Ge quantum well confined by the epitaxial Si shell, where CB is the conduction band and VB is the valence band. The dashed line indicates the Fermi level, E_F. (b) G-V_g recorded at different temperatures on a 400 nm long top-gated device; the red, blue, green, and black curves correspond to temperatures of 5 K, 10 K, 50 K, and 100 K, respectively. Insets show a schematic and scanning electron micrograph of a top-gated NWFET; scale bar is 500 nm. (c) Transconductance dG/dV_g as a function of V_{sd} and V_g. Dashed lines are guides indicating the evolution of conductance modes with V_{sd} and V_g. The vertical arrows highlight values of subband spacings $\Delta E_{1,2}$ and $\Delta E_{2,3}$, respectively. (d) I_{ds}-V_g data for a Ge/Si NWFET (190 nm channel length, 4 nm HfO_2 dielectric) with blue, red, and green data points corresponding to V_{ds} values of -1 V, -0.1 V, and -0.01 V, respectively; inset shows the linear scale plot of I_{ds}-V_g measured at V_{ds} = -1 V. (e) Intrinsic delay, τ, versus channel length for seven different Ge/Si nanowire devices with HfO_2 dielectric (open circle) and ZrO_2 dielectric (open square). (Reprinted with permission from[44,45]. © 2005 National Academy of Sciences USA and 2006 Nature Publishing Group, respectively.)

nanoelectronics, and to explore the fundamental properties of both one-dimensional electron and hole gases. Our designed NW structure consists of an intrinsic GaN core and sequentially deposited undoped AlN and AlGaN shells (Fig. 9a), where the epitaxial AlN interlayer is used to reduce alloy scattering from the AlGaN outer shell and to provide a larger conduction band discontinuity for better electron confinement[46]. Notably, temperature-dependent transport data confirm the accumulation of an electron gas in undoped GaN/AlN/$Al_{0.25}Ga_{0.75}N$ NWs, and yield an intrinsic electron mobility of 3100 cm^2/Vs at room temperature that reaches 21 000 cm^2/Vs at 5 K (Fig. 9b), where the increased mobility at low temperature is consistent with reduced phonon scattering of the electron gas. The room-temperature value is comparable to the record value in planar GaN/AlGaN heterostructures, and substantially higher than values obtained in *n*-type GaN NWs. In addition, top-gated FETs fabricated

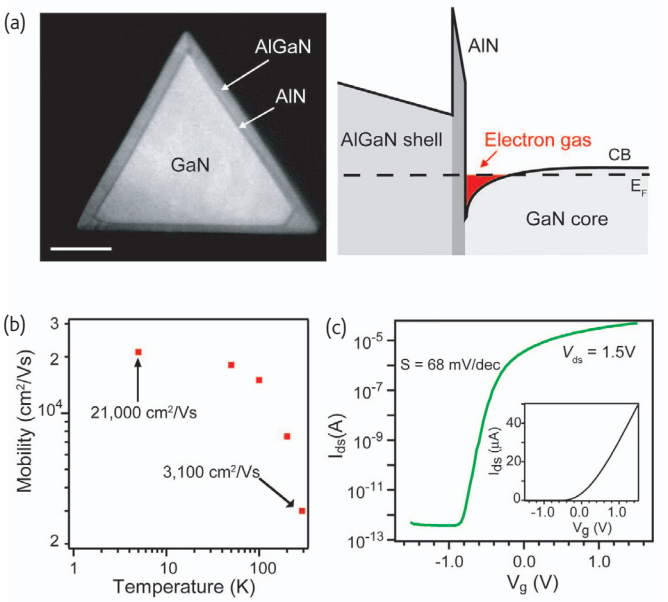

Fig. 9 GaN/AlN/AlGaN radial heterostructure NWFETs. (a, left) Cross-sectional, high-angle annular dark-field scanning TEM image of a GaN/AlN/AlGaN radial nanowire heterostructure; scale bar is 50 nm. (a, right) Band diagram of a dopant-free GaN/AlN/AlGaN NW illustrating the formation of an electron gas (red region) at the core-shell interface confined by the epitaxial AlN/AlGaN shells. (b) Plot of the intrinsic electron mobility of a GaN/AlN/$Al_{0.25}Ga_{0.75}N$ NWFET as a function of temperature, where the values were obtained after the correction for contact resistance. (c) Logarithmic scale I_{ds}-V_g curve recorded at V_{ds} = 1.5 V, on a top-gated GaN/AlN/$Al_{0.25}Ga_{0.75}N$ NWFET (channel length 1 μm, 6 nm ZrO_2 dielectric); inset shows the linear scale plot of the same data. (Reprinted with permission from[46]. © 2006 American Chemical Society.)

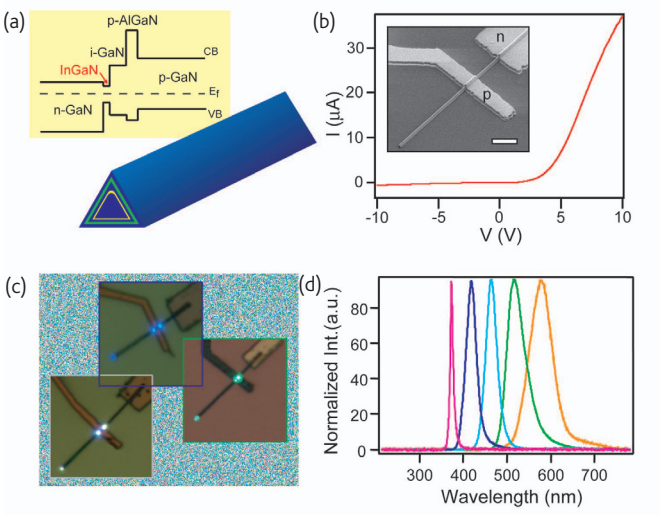

Fig. 10 Multicolor III-nitride CMS NW LEDs. (a) Schematic and corresponding band diagram for an n-GaN/InGaN/GaN/p-AlGaN/p-GaN CMS nanowire. The InGaN and AlGaN shells are highlighted with yellow and green colors, respectively. (b) I-V data recorded from a typical CMS NW device with contacts to the n-core and p-shell. Inset shows a scanning electron micrograph of the device; scale bar is 2 μm. (c) EL images of three forward-biased CMS NW LEDs with ~15%, 30%, and 35% In, showing blue, greenish-blue, and greenish-yellow emission, respectively. (d) Normalized EL spectra recorded from five multicolor CMS NW LEDs with 1%, 10%, 20%, 25%, and 35% In (left to right), respectively. (Reprinted with permission from[41,42]. © 2004 and 2005 American Chemical Society.)

with these NW radial heterostructures exhibit scaled transconductance (420 mS/μm) and subthreshold slope (68 mV/dec) values (Fig. 9c) that are substantially better than previous *n*-channel NWFETs. Taken together, these results testify to the functional advantage of developing more complex building blocks like these radial nanowire heterostructures.

Radial NW heterostructures for photonics

The radial NW concept also offers substantial opportunities for NW optoelectronics since the required *n*- and *p*-type active materials can be incorporated as the core and shell, which enables carrier injection or collection over a much larger area than possible in crossed NW devices and axial NW heterostructures. We first demonstrated a general strategy for realizing these structures through the synthesis of well-defined doped III-nitride-based core-multishell (CMS) NW heterostructures (Fig. 10a)[41,42]. In these materials, an *n*-type GaN core and *p*-type GaN outer shell serve as electron and hole injection layers, an $In_xGa_{1-x}N$ shell provides a tunable band gap quantum well for efficient radiative recombination of injected carriers, and an AlGaN shell is incorporated to enhance confinement of both carriers and photons in the InGaN active layer. Current versus voltage characteristics of CMS NW devices with separate contacts to the *n*-type core and *p*-type outer shell show the expected *p*-*n* diode current rectification (Fig. 10b). In forward bias, the devices yield strong light emission with the LED color dependent on the In composition, defined during synthesis, in the CMS NW heterostructure (Fig. 10c). Significantly, LED spectra collected from CMS NW devices with intentionally increasing In composition demonstrate a systematic red-shift of the emission from 367 nm to 577 nm, covering the short wavelength region of the visible spectrum. Notably, preliminary data recorded from these new CMS structures exhibit an external quantum efficiency that is comparable to InGaN-based single-quantum-well thin-film LEDs at similar emission wavelengths[65] and substantially better than previous crossed NW LEDs. The efficient injection and radiative recombination of carriers, as well as synthetically tunable emission wavelength of these radial NW devices, represent a clear advance in nanoLED sources and thus a promising pathway to multicolor NW injection lasers in the future.

Concluding remarks

We have shown that semiconductor NWs offer many opportunities for the assembly of nanoscale electronic and optoelectronic devices and arrays by the bottom-up paradigm. Central to our progress in the field

and future efforts at realizing applications has been the rational control of key NW parameters during growth, including chemical composition, structure, size, morphology, and doping, since it is these parameters that determine predictable device function. The examples described here illustrate how, with increasing control over the parameters of the basic NW building blocks from homogenous doped materials to increasingly complex axial and radial heterostructures, it has been possible to demonstrate key advantages of NWs in electronics and photonics compared with conventional technologies. Integration strategies have also been developed that remove the constraints of lithography facing conventional top-down technologies today. Looking into the future, we believe that continued advances in our capability to control the structural/compositional complexity of NWs during growth, which correspondingly determines the functional complexity of the building blocks, together with advances in organizing them into larger integrated arrays, will lead to increasingly unique nanoelectronic and optoelectronic circuits and systems that will create the technologies of the future. mt

Acknowledgments

We thank Gengfeng Zheng, Song Jin, Dongmok Whang, Zhaohui Zhong, Ying Fang, Robin Friedman, Michael McAlpine, Fernando Patolsky, Deli Wang, Yu Huang, Xiangfeng Duan, Oliver Hayden, Ritesh Agarwal, Mark Gudiksen, Lincoln Lauhon, Yue Wu, Chen Yang, Wei Lu, and Silvija Gradecak for contributions to the work presented in this article. Charles Lieber acknowledges generous support of this work by Defense Advanced Research Projects Agency, Air Force Office of Scientific Research, Intel, National Science Foundation, Applied Biosystems, and Samsung.

REFERENCES

1. Hu, J., *et al., Acc. Chem. Res.* (1999) **32**, 435
2. Lieber, C. M., *MRS Bull.* (2003) **28** (7), 486
3. Cui, Y., *et al.*, In: *Nanowires and Nanobelts – Materials, Properties and Devices*, Wang, Z. L., (ed.) Kluwer Academic Publishers (2003), 3
4. Huang, Y., and Lieber, C. M., *Pure Appl. Chem.* (2004) **76**, 2051
5. Lauhon, L., *et al., Philos. Trans. R. Soc. London, Ser. A* (2004) **362**, 1247
6. Samuelson, L., *Materials Today* (2003) **6** (10), 22
7. Xia, Y., *et al., Adv. Mater.* (2003) **15**, 353
8. Wang, Z. L., *Materials Today* (2004) **7** (6), 26
9. Bruchez, M., *et al., Science* (1998) **281**, 2013
10. Murray, C. B., *et al., Ann. Rev. Mater. Sci.* (2000) **30**, 545
11. Wang, X., *et al., Nature* (2005) **437**, 121
12. Odom, T., *et al., J. Phys. Chem. B* (2000) **104**, 2794
13. Ouyang, M., *et al., Acc. Chem. Res.* (2002) **35**, 1018
14. Ouyang, M., *et al., Annu. Rev. Phys. Chem.* (2002) **53**, 201
15. Yao, Z., *et al.*, In: *Carbon Nanotubes: Synthesis, Structure, Properties and Applications*, Dresselhaus, M. S., *et al.*, (eds.), Springer, New York (2000), 147
16. Liu, J., *et al., MRS Bull.* (2004) **29** (4), 244
17. McEuen, P. L., and Park, J. Y., *MRS Bull.* (2004) **29** (4), 272
18. Morales, A. M., and Lieber, C. M., *Science* (1998) **279**, 208
19. Levitt, A. P., (ed.), *Whisker Technology*, Wiley, New York (1970)
20. Wagner, R. S., and Ellis, W. C., *Appl. Phys. Lett.* (1964) **4**, 89
21. Duan, X. F., and Lieber, C. M., *Adv. Mater.* (2000) **12**, 298
22. Cui, Y., *et al., J. Phys. Chem. B* (2000) **104**, 5213
23. Duan, X. F., and Lieber, C. M., *J. Am. Chem. Soc.* (2000) **122**, 188
24. Duan, X. F., *et al., Appl. Phys. Lett.* (2000) **76**, 1116
25. Gudiksen, M., and Lieber, C. M., *J. Am. Chem. Soc.* (2000) **122**, 8801
26. Wang, J., *et al., Science* (2001) **293**, 1455
27. Duan, X. F., *et al., Nature* (2001) **409**, 66
28. Gudiksen, M., *et al., J. Phys. Chem. B* (2001) **105**, 4062
29. Huang, Y., *et al., Nano Lett.* (2002) **2**, 101
30. Cui, Y., *et al., Nano Lett.* (2003) **3**, 149
31. Zhong, Z., *et al., Nano Lett.* (2003) **3**, 343
32. Barrelet, C. J., *et al., J. Am. Chem. Soc.* (2003) **125**, 11498
33. Greytek, A. B., *et al., Appl. Phys. Lett.* (2004) **84**, 4176
34. Wu, Y., *et al., Nano Lett.* (2004) **4**, 433
35. Zheng, G., *et al., Adv. Mater.* (2004) **16**, 1890
36. Radovanovic, P. V., *et al., Nano Lett.* (2005) **5**, 1407
37. Gudiksen, M., *et al., Nature* (2002) **415**, 617
38. Wu, Y., *et al., Nature* (2004) **430**, 61
39. Yang, C., *et al., Science* (2005) **310**, 1304
40. Lauhon, L., *et al., Nature* (2002) **420**, 57
41. Qian, F., *et al., Nano Lett.* (2004) **4**, 1975
42. Qian, F., *et al., Nano Lett.* (2005) **5**, 2287
43. Hayden, O., *et al., Adv. Mater.* (2005) **17** 701
44. Lu, W., *et al., Proc. Natl. Acad. Sci. USA* (2005) **102**, 10046
45. Xiang, J., *et al., Nature* (2006) **441**, 489
46. Li, Y., *et al., Nano Lett.* (2006) **6**, 1468
47. Jin, S., *et al., Nano Lett.* (2004) **4**, 915
48. Bryllert, T., *et al., IEEE Electron Device Lett.* (2006) **27**, 323
49. Doh, Y., *et al., Science* (2005) **309**, 272
50. Zhong, Z., *et al., Nano Lett.* (2005) **5**, 1143
51. Tilke, A., *et al., J. Appl. Phys.* (2001) **89**, 8159
52. McAlpine, M. C., *et al., Nano Lett.* (2003) **3**, 443
53. Friedman, R. S., *et al., Nature* (2005) **434**, 1085
54. Cui, Y., *et al., Science* (2001) **293**, 1289
55. Hahm, J., and Lieber, C. M., *Nano Lett.* (2004) **4**, 51
56. Patolsky, F., *et al., Proc. Natl. Acad. Sci. USA* (2004) **101**, 14017
57. Wang, W. U., *et al., Proc. Natl. Acad. Sci. USA* (2005) **102**, 3208
58. Zheng, G., *et al., Nat. Biotechnol.* (2005) **23**, 1294
59. Patolsky, F., and Lieber, C. M., *Materials Today* (2005) **8** (4), 20
60. Huang, Y., *et al., Science* (2001) **294**, 1313
61. Zhong, Z., *et al., Science* (2003) **302**, 1377
62. Huang, Y., *et al., Small* (2005) **1**, 142
63. Duan, X. F., *et al., Nature* (2003) **421**, 241
64. Hayden, O., *et al., Nat. Mater.* (2006) **5**, 352
65. Mukai, T., *IEEE J. Sel. Top. Quantum Electron.* (2002) **8**, 264